Hindawi
Advances in Materials Science and Engineering
Volume 2020, Article ID 4849038, 11 pages
https://doi.org/10.1155/2020/4849038

Research Article

Study on Corrosion Characteristics of Concrete-Filled CFRP-Steel Tube Piles under Hygrothermal Environment

Honghan Dong[1,2] **Yujue Zhou,**[3] **and Ning Zhuang**[2]

[1]*Department of Civil Engineering, MOE Key Laboratory of Soft Soils and Geoenvironmental Engineering, Zhejiang University, Hangzhou 310058, China*
[2]*Jiangsu Key Laboratory of Coast Ocean Resources Development and Environment Security, Hohai University, Nanjing 210098, China*
[3]*College of Civil Engineering, Tongji University, Shanghai 200092, China*

Correspondence should be addressed to Ning Zhuang; zhuangning1977@163.com

Received 3 September 2019; Revised 27 December 2019; Accepted 29 January 2020; Published 25 February 2020

Academic Editor: Aniello Riccio

The corrosion damage of pile foundations caused by a hygrothermal environment is a significant factor that influences the service life of high-pile wharf structures. The concrete-filled CFRP-steel tube (CFRP-CFST) pile is a composite structure composed of external Carbon Fiber-Reinforced Polymer (CFRP) sheets and inner concrete-filled steel tubes. It has a high-bearing capacity and excellent corrosion resistance and is an ideal structure for pile foundations in aggressive environments. In this paper, twelve CFRP-CFST pile specimens with diameters of 114 mm and heights of 1200 mm and another forty-two CFRP-steel plate specimens with CFRP widths of 30–50 mm were built. A high hot and humid environment simulation system was designed to conduct corrosion experiments with these specimens. At different theoretical corrosion degrees, the half-cell potential, corrosion products, corrosion expansion, and adhesive property were investigated. The test results showed an obvious increase in the mechanical properties and corrosion resistance when the concrete-filled steel tube was externally bonded to CFRP sheets. The experimental results show that the CFRP-CFST pile is an effective way to protect piles from corrosion and can be widely used for high-pile wharfs in aggressive environments.

1. Introduction

The concrete-filled steel tube (CFST) pile is a widely used composite structure. Concrete has excellent compressive resistance but poor tensile resistance [1]. Steel tubes have excellent flexural properties but easily succumb to buckling failure under high pressure. The strength and ductility of CFST piles may rapidly decrease due to material corrosion in hot and humid environments. CFRP composites are considered as a new material to overcome the weakness of CFST piles due to their higher strength, favorable strength-to-weight ratio, and excellent corrosion resistance. This has resulted in the appearance of a new structure, the concrete-filled CFRP-steel tube (CFRP-CFST) pile, which has a high-bearing capacity and excellent corrosion resistance. Externally bonded CFRP sheets can apply circular pressure to constrain concrete and steel tube deformation and improve the mechanical behaviors of CFRP-CFST piles. CFRP sheets also have excellent durability to effectively prevent the erosion of corrosive media under hygrothermal environments [2]. In addition, CFRP can directly reduce the amount of steel material and the construction difficulty [3].

The CFRP-CFST pile of high-pile wharfs has three corrosion zones: the atmospheric zone, the dry and wet alternating zone, and the underwater zone. Oxygen and water are indispensable for the occurrence and development of corrosion [4–7]. The underwater zone lacks enough oxygen, and the water supply in the atmospheric zone is insufficient. Therefore, the dry and wet alternating zone is mostly prone to corrosion because it is wetted periodically

by tidal levels and has an adequate supply of water and oxygen. For CFRP-CFST piles, the internal steel pipe will be corroded quickly when the outer CFRP sheet is penetrated by the corrosion medium. This will seriously reduce the bearing capacity and service life of the CFRP-CFST pile. At present, studies have mainly focused on the mechanical properties of CFRP-CFST piles [8]. For example, some static load experiments have been conducted to investigate the axial and flexural behavior of CFRP-CFST piles [9–11]. The studies reported that externally bonded CFRP would improve the bearing capacity and ductility to certain degrees. Based on the limit equilibrium theory, a formula for calculating the bearing capacity of damaged CFRP-CFST members before and after compression was presented, and the calculated results were in good agreement with experimental data [12–15]. Other tests showed that the failure pattern was steel tube buckling, and CFRP was pulled off under static loading [16]. The bending, shear, and torsion properties were related to the bonding direction and number of CFRP bonding layers [17].

In addition to the above studies, experiments have been conducted to investigate the improvement of the mechanical properties of piles [18]. However, little information has been found in the literature regarding the corrosion properties of CFRP-CFST piles under the hygrothermal environment of the ocean [19]. Therefore, the main objective of this study is to research the corrosion characteristics of CFRP-CFST piles under the hot and humid environments.

2. Experimental Program

2.1. Test Program. Twelve CFRP-CFST pile specimens were built (Figure 1) in the laboratory. Each pile specimen was divided into three zones: an atmospheric zone, a dry and wet alternating zone, and an underwater zone, as shown in Figure 2. All pile specimens were divided into three groups, and each group included four pile specimens according to the degree of corrosion (0%, 5%, 10%, and 15%), as summarized in Table 1. The geometric parameters of the pile specimens are shown in Table 2. Each pile specimen was mounted with nine strain gauges to monitor the deformation caused by the expansion of corrosion, as shown in Figure 2. The surface of the pile was covered with CFRP sheets, leaving no gaps. It was necessary to polish the surface of the steel pipes with an angle mill before pasting the CFRP sheets. After that, the entire outer surface of the steel pipe was repeatedly wiped with a nonwoven cloth and soaked in an acetone solution to remove the moisture and dust from the surface of the steel pipe. Then, the CFRP sheets were pasted from the bottom to the top of a pile, and the lap width between the adjacent layers was not less than 15 cm. Finally, the outer surface of the CFRP sheets was coated with glue, and the specimens were left in a cool and ventilated place for over 24 hours.

2.2. Material Properties. The concrete mix proportion by weight was aggregate : sand : water : cement = 2.20 : 1.35 : 1.00 : 0.35. As the pile foundation model was constructed, standard test blocks (10 mm × 10 mm × 10 mm) for testing the compressive strength of the concrete were made. The concrete pouring process was continuous. No concrete was poured into a space of approximately 2 cm from the top of the steel tube to facilitate the connection of the power supply during the accelerated corrosion test. Before the

Figure 1: CFRP-CFST pile specimens.

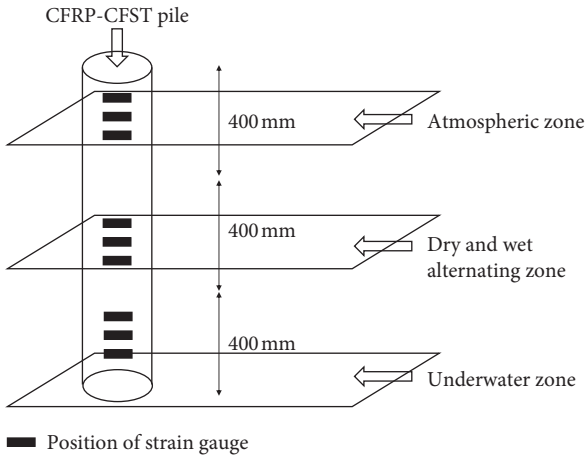

Figure 2: Corrosion zones of pile.

Table 1: Test program.

Groups of CFRP-CFST pile	Corrosion degree (% mass loss)			
	0	5%	10%	15%
Without CFRP	U-0	U-5	U-10	U-15
One layer of CFRP	P1-0	P1-5	P1-10	P1-15
Two layers of CFRP	P2-0	P2-5	P2-10	P2-15

Table 2: Geometric parameters of pile specimens.

	Height (mm)	Cross section diameter (mm)	Steel tube thickness (mm)
Pile specimens	1200	114	2.7

ballast tests, it was necessary to use plastering mortar for supplementary casting. The concrete had an average 28-day compressive strength of 36.6 MPa based on compressive strength tests [20]. The yield strength of the steel tube was 235 MPa based on tensile tests. The main properties of the CFRP sheets and the epoxy resin adhesive are shown in Tables 3 and 4, respectively, according to the factory standards. The epoxy resin adhesive was composed of grade A and grade B of glue. The two grades were mixed at a mass ratio of 3 : 1 with a hand-held electric mixer to a uniform state when used [21].

2.3. Preparing the Test. CFRP-CFST pile specimens were kept in the tank (Figure 3) and subjected to wet-dry cycles by high chloride seawater, the chemical composition of which is shown in Table 5. The tank was in the room and kept at room temperature. The difference between high and low tides was 400 mm, and the water level was changed gradually every 12 hours using a water pump and a floating switch to simulate the tidal range zone, as shown in Figure 4. The water level circulation system used a remote automatic control, and water was replenished regularly to make up for evaporation [22].

To achieve corrosion within a reasonable time, the accelerated corrosion technique based on Faraday's law was used in the laboratory. In this technique, a constant current system is built, and a DC galvanostatic power supply is used to provide the desired current (Figure 3). The current in the experiment was set as 166 mA. The time required for various degrees of corrosion was calculated based on Faraday's law [23, 24]. Faraday's law along with the induced current calculations is presented in the following:

$$m_1 = \frac{M \cdot i \cdot S_a \cdot T}{ZF}, \quad (1)$$

where m_1 is weight of steel consumed; M is atomic weight of metal (56 g for Fe); i is current density level; T is time; Z is ionic charge ($Fe \longrightarrow Fe^{2+} + 2e^{-}$) = 2; F is Faraday's constant; and S_a is surface zone of the corroded steel.

3. Experimental Results and Discussions

3.1. Half-Cell Potential. The half-cell potential measurement is one of the most widely used nondestructive methods to monitor and assess corrosion. In essence, the measured potential value is the internal potential difference of the microsection of the steel tube. This potential difference will generate a weak current in the microsection of the steel tube, which leads to electrochemical corrosion. Compared to other methods such as the rotating disk electrode (RDE), the half-cell potential measurement has its own advantages. It is possible and sensitive to examine the small current inside the steel cube even at the common fuel cell working ranges. In addition, it is easy to operate and measure the same position repeatedly to obtain the average value and thus ensure a relatively high accuracy of the results.

In this paper, the CANIN + corrosion detector was chosen as the electric potential measuring instrument [25]. To detect the potential values, the Cu-$CuSO_4$ solution and the pile specimens were combined to form a battery system. Once the steel tube was corroded and the charge was exchanging, the current and polarization occurred on the contact surface. During polarization, the metal anode potential increased, and the cathode potential decreased until the potential was balanced. It is generally agreed that the half-cell potential measurements can be interpreted according to Table 6 [26].

The half-cell potential values of the CFRP-CFST pile specimens were increased with the degree of corrosion, as shown in Figure 5. The average potential of the dry and wet alternating zone was smaller than that of the other corrosion zones. This indicated that the dry and wet alternating zone was in a more active corrosion state because it had sufficient oxygen and water. For the pile specimens (U-0, U-5, U-10, and U-15) without CFRP sheets, the average electric potential values corresponding to different corrosion degrees (0%, 5%, 10%, and 15%) in the dry and wet alternating zone were −80 mV, −349 mV, −639 mV, and −709 mV, respectively. This showed that the pile specimens were in the corrosion state from the corrosion degree of 5%.

For piles specimens (P1-5, P1-10, and P1-15) with one layer of CFRP sheets, the half-cell potential values significantly decreased. The average half-cell potential values corresponding to different corrosion degrees (5%, 10%, and 15%) in the dry and wet alternating zone were −157 mV, −403 mV, and −432 mV, respectively, which were approximately 55%, 33%, and 39% more positive compared to the piles specimens without CFRP sheets. The potential value showed that the dry and wet alternating zone had a greater than 90% probability of no active corrosion at 5%. The half-cell potential values of piles specimens P1-10 and P1-15 were very close when the corrosion degree was at the high levels of 10% and 15%. The CFRP sheet of the CFRP-CFST pile specimens could prevent the penetration of the corrosive medium, which delayed the corrosion of the piles, particularly at high degrees of corrosion.

For pile specimens (P2-0, P2-5, and P2-15) with two layers of CFRP sheets, their half-cell potential values were all smaller than those with one layer of CFRP sheets. However, their change trends were identical. The corrosion potentials in the dry and wet alternating zone were −157 mV, −200 mV, and −246 mV, respectively, which were 63%, 70%, and 65% more positive compared with the piles specimens without CFRP sheets at corrosion degrees of 5%, 10%, and 15%, respectively. This indicated that the electric potential of the piles would decrease as the number of layers of CFRP sheets

Table 3: Properties of CFRP.

Thickness (mm)	Tensile strength (MPa)	Elasticity modulus (MPa)	Ductility (%)	Density (g/cm^3)	Tensile strain ($\times 10^{-6}$)
0.11	3450	2.3×10^5	2.1	1.8	16650

Table 4: Properties of the epoxy resin adhesive.

Compressive strength (MPa)	Tensile strength (MPa)	Shear strength (MPa)	Elasticity modulus (MPa)
64.6	25.9	20.8	5.6×10^3

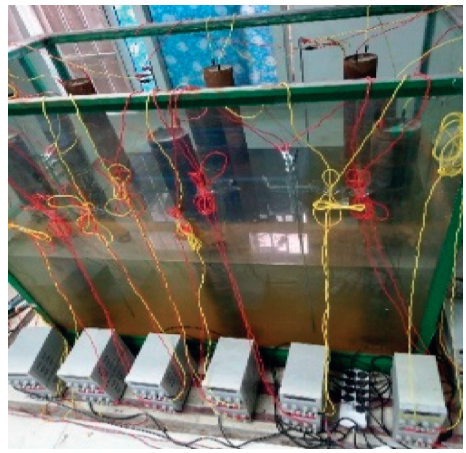

Figure 3: Simulated environment and accelerating corrosion system.

Table 5: Chemical composition of seawater.

Chemical compound	Concentration (g/L)	Chemical compound	Concentration (g/L)
NaCl	24.53	$NaHCO_3$	0.201
$MgCl_2$	5.2	KBr	0.101
Na_2SO_4	4.09	H_3BO_3	0.027
$CaCl_2$	1.16	$SrCl_2$	0.025
KCl	0.695	NaF	0.003

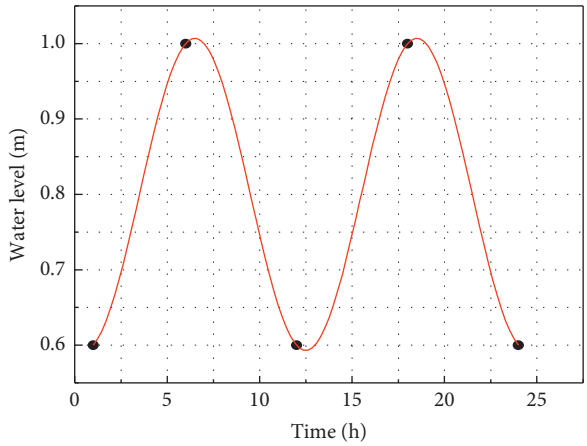

Figure 4: Simulated sea tidal cycles.

increased. The CFRP sheet had a significant effect on delaying the corrosion degree of the CFRP-CFST pile specimens.

3.2. Corrosion Expansion. As the steel tube of the CFRP-CFST pile specimens corroded, the rust expanded more than six times in volume compared with the steel. The accumulation of products would produce the expansion stress that caused the surface strain of the CFRP-CFST pile specimens. The arrangement of the strain gauges is shown in Figure 2. These strain gauges were applied to the surface of the CFRP, leaving no gaps, to measure the circumferential microstrain of the model piles at the specified time node. They were arranged horizontally around the piles. Strain data were collected for increments of 5% in the theoretical corrosion rate.

As shown in Figure 6, the strains of the dry and wet alternating zone were more severe than those of the atmospheric zone and underwater zone, which was consistent with the variation of the half-cell potentials. This also indicated that the dry and wet alternating zone was the most prone to corrosion.

The CFRP sheet could apply a constraining force to limit corrosion expansion during the corrosion stage. For the pile specimens with two CFRP layers, the maximum strain of the

Table 6: Dependence between potential and corrosion probability.

Potential	Probability of corrosion
$E_{cor} < -350$ mV	Greater than 90% probability that corrosion is occurring
-350 mV $\leq E_{cor} \leq -200$ mV	Corrosion activity is uncertain
$E_{cor} < -200$ mV	90% probability that no corrosion is occurring (10% risk of corrosion)

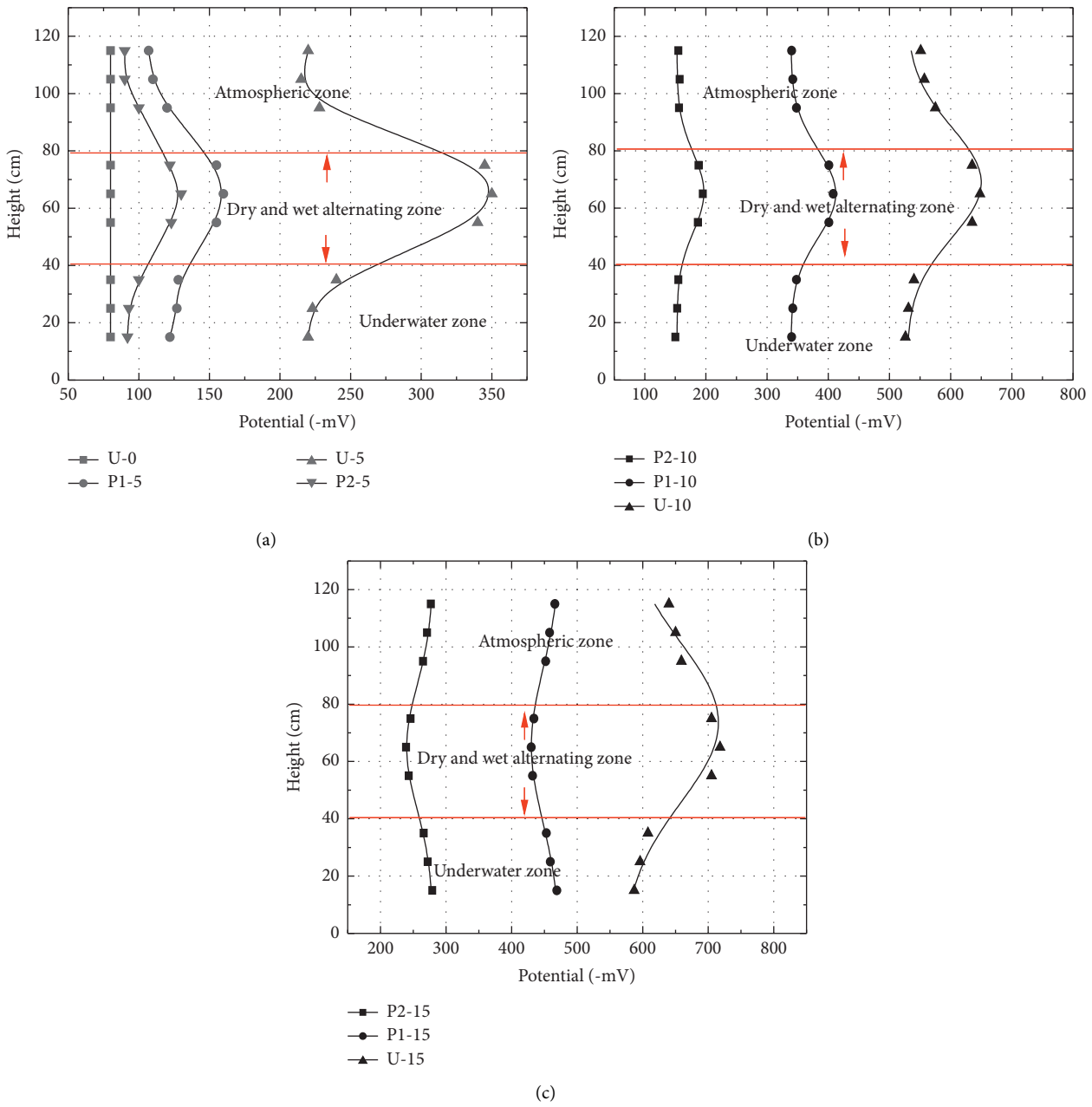

Figure 5: Measured half-cell potentials of pile specimens: (a) 5% corrosion degree, (b) 10% corrosion degree, and (c) 15% corrosion degree.

dry and wet alternating zone was approximately 18%, 19%, and 26% smaller than that of the specimens with one CFRP layer and 28%, 31%, and 37% smaller than that of the specimens with no CFRP layer at corrosion degrees of 5%, 10%, and 15%, respectively. The strains of the piles would decrease as the number of CFRP sheet layers increased. The higher the lever of the corrosion degree, the clearer the effects.

3.3. Corrosion Products. The composition of steel corrosion products has been studied by many scholars. Research on the corrosion products of iron and steel began with Evans' local battery theory in 1932 [27]. Then, the composition and structural changes of steel corrosion products were studied by many Japanese scholars during the period from 1940 to 1960 [28]. After that, the electrochemical reaction model and

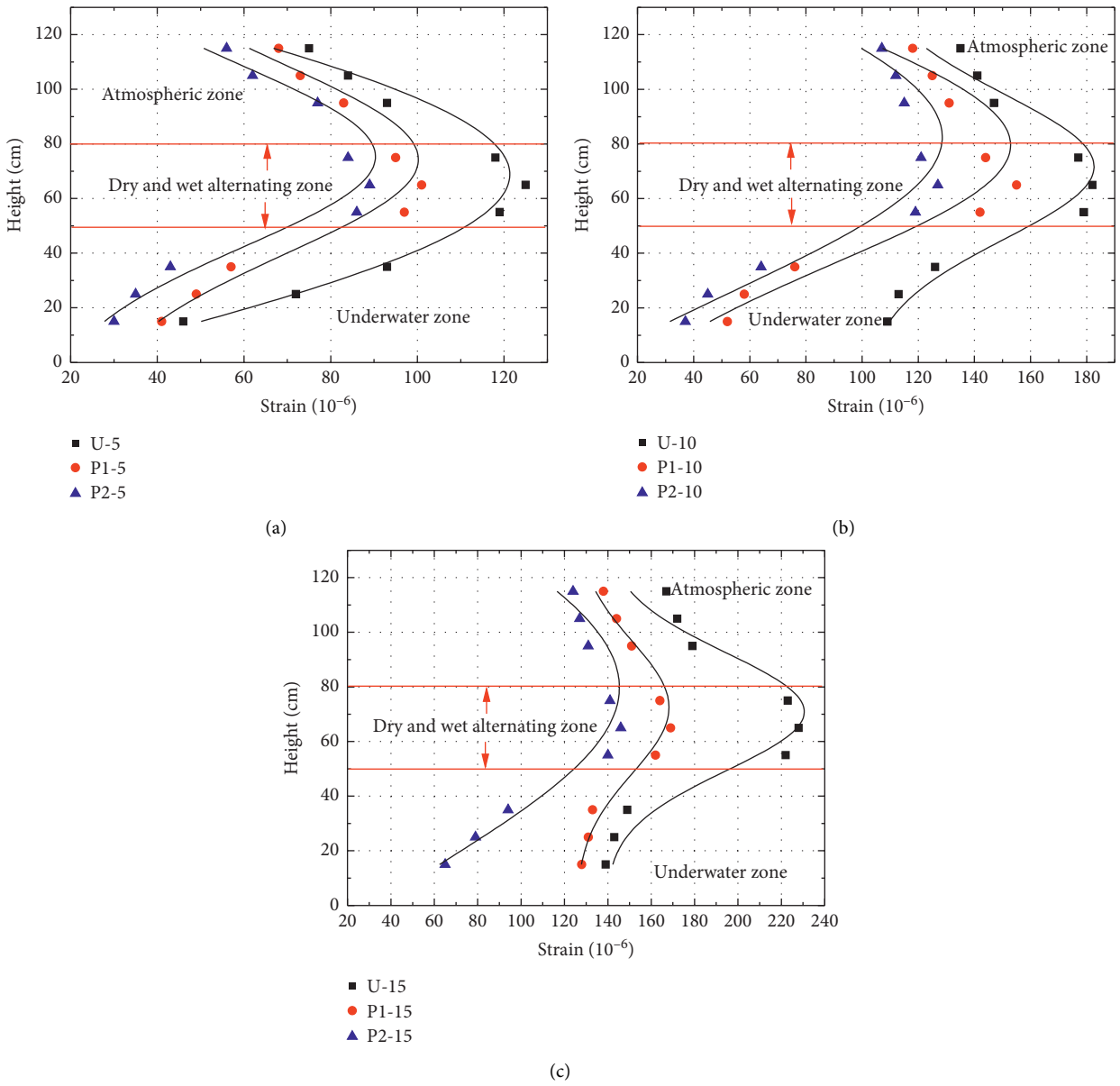

Figure 6: Strains of piles at different corrosion degrees: (a) 5% corrosion degree, (b) 10% corrosion degree, and (c) 15% corrosion degree.

the potential-pH diagram of FeOOH appeared in 1973 [29]. Now, X-ray diffraction analysis (XRD) is treated as an effective method. When an X-ray with a certain wavelength is irradiated on the surface of a crystalline material, the X-ray is blocked by the rehearsed regular particles and scattered. Due to the corresponding and unique radiation reaction of the crystal itself, the phase of the scattered ray is strengthened in certain directions. In this paper, XRD was used to analyze the crystal formation of the corrosion products of the model piles at different corrosion stages [30].

The corrosion composition and the corrosion-induced expansion were different during the corrosion stages. The mechanism of steel tube corrosion products is shown in Figure 7 [31]. The element of Fe on the surface of the steel matrix would first precipitate as green Fe^{2+} or $FeOH^{+}$ and then oxidize into γ-FeOOH or α- FeOOH. At the same time, Fe_3O_4 can also be produced. Through analyzing the components of the corrosion products at different stages of pile corrosion, we can fundamentally and indirectly verify the degree of corrosion. Additionally, it is beneficial to develop effective reinforcement schemes with CFRP sheets, especially for structures that have been in service for a certain number of years.

The X-ray diffraction patterns of the dry and wet alternating zone at 5% and 10% corrosion degrees are shown in Figure 8. The diffraction peaks were concentrated at angles of $2\theta = 26.75^{\circ}$, $2\theta = 35.71^{\circ}$, $2\theta = 45.15^{\circ}$, $2\theta = 46.35^{\circ}$, and $2\theta = 62.24^{\circ}$, especially at angles of $2\theta = 26.75^{\circ}$ and $2\theta = 35.75^{\circ}$ at a 10% corrosion degree. The corresponding components of these characteristic peaks were mainly Fe_2O_3, Fe_3O_4, α- FeOOH, and γ-FeOOH. As the number of CFRP sheet layers increased, the peak diffraction tended to shift to

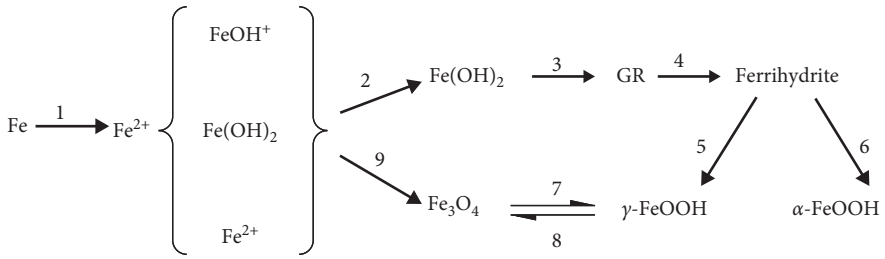

Figure 7: Mechanism of the corrosion products of a steel pipe.

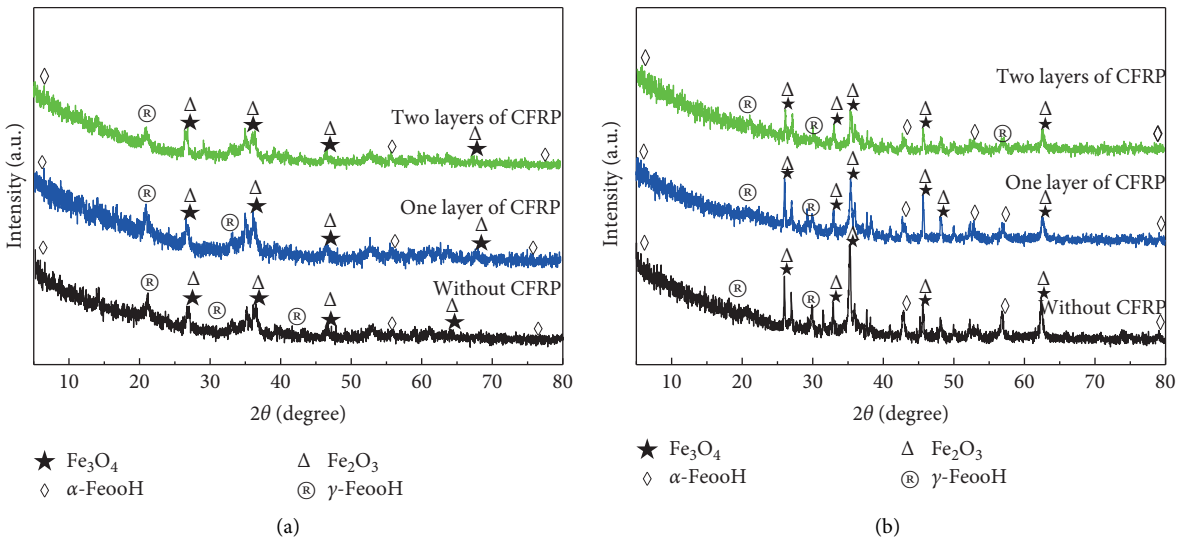

Figure 8: XRD pattern of corrosion products: (a) 5% corrosion degree and (b) 10% corrosion degree.

the left; that is to say, the angle of the diffraction peaks became smaller. At the same time, the height of the diffraction peaks also decreased. It was also concluded from Figure 8 that the number of diffraction peaks decreased as the number of CFRP sheet layers increased, indicating that an increase in the number of CFRP sheet layers could slow the degree of corrosion of pile specimens because CFRP sheets prevent the invasion of aggressive media. On the other hand, the property of α- FeOOH that was stable and had a low electrochemical activity was on the outside part of the rust layer, which acted as a certain isolation layer [32]. The diffraction peaks appeared at angles of $2\theta = 21.25^{\circ}$, $2\theta = 26.15^{\circ}$, $2\theta = 36.74^{\circ}$, $2\theta = 47.15^{\circ}$, and $2\theta = 64.04^{\circ}$ at a 5% corrosion degree. The corresponding components of these characteristic peaks were the same as those for a 10% corrosion degree. Unlike the 10% corrosion degree, the diffraction peaks of α-FeOOH and γ-FeOOH were smaller, which indicated a lower corrosion degree.

3.4. Bond Performance between CFRP and Steel Tubes. The bond between the CFRP and the steel pipe is the weakest part that has a direct impact on the mechanical properties of piles, and the strength of the bond property directly affects the reinforcement effect of CFRP. In addition, the bond is the last defense once the carbon fiber is broken down by corrosive ions during the service of the piles. It is necessary to study the bond properties between the CFRP and the steel tubes [33].

To study the bond performance between the CFRP and the steel tubes in the piles, three groups of CFRP-steel plate specimens were prepared and corroded in the dry and wet alternating zone, as shown in Table 7. The dimensions of the steel plate were as follows: 220 mm in length, 70 mm in width, and 3 mm in thickness (Figure 9). The properties of the steel plate were the same as those of the steel tubes of the CFRP-CFST pile. To eliminate the effect of width on the results, the CFRP widths were set to 30 mm, 40 mm, and 50 mm. An accelerated corrosion technique based on Faraday's law was also used to corrode the CFRP-steel plates. The load-displacement test of the CFRP-steel plate specimens was carried out on a universal test machine with displacement control. The steel plate was connected to the aluminum plate with CFRP sheets of different widths (Figure 9). Successive loads were applied in stages on both ends of the specimen until apparent slip appeared. The strain gauges were pasted on the middle surface of the CFRP sheets. The data of the corresponding loads were recorded for every 0.05 mm of displacement.

The bond force to displacement of the pile specimens was linear as shown in Figure 10. The maximum bond force decreased as the corrosion degree increased. As the width of

Table 7: CFRP-steel plate specimens.

Groups	CFRP width (mm)	CFRP layers	Corrosion degree						
			0%	2.5%	5%	7.5%	10%	12.5%	15%
One	30	One	A1-0	A1-2.5	A1-5	A1-7.5	A1-10	A1-12.5	A1-15
		Two	A2-0	A2-2.5	A2-5	A2-7.5	A2-10	A2-12.5	A2-15
Two	40	One	B1-0	B1-2.5	B1-5	B1-7.5	B1-10	B1-12.5	B1-15
		Two	B2-0	B2-2.5	B2-5	B2-7.5	B2-10	B2-12.5	B2-15
Three	50	One	C1-0	C1-2.5	C1-5	C1-7.5	C1-10	C1-12.5	C1-15
		Two	C2-0	C2-2.5	C2-5	C2-7.5	C2-10	C2-12.5	C2-15

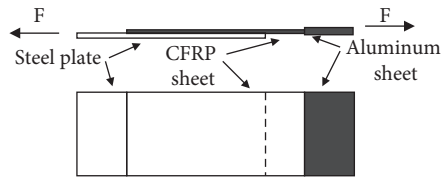

Figure 9: CFRP-steel plate specimens.

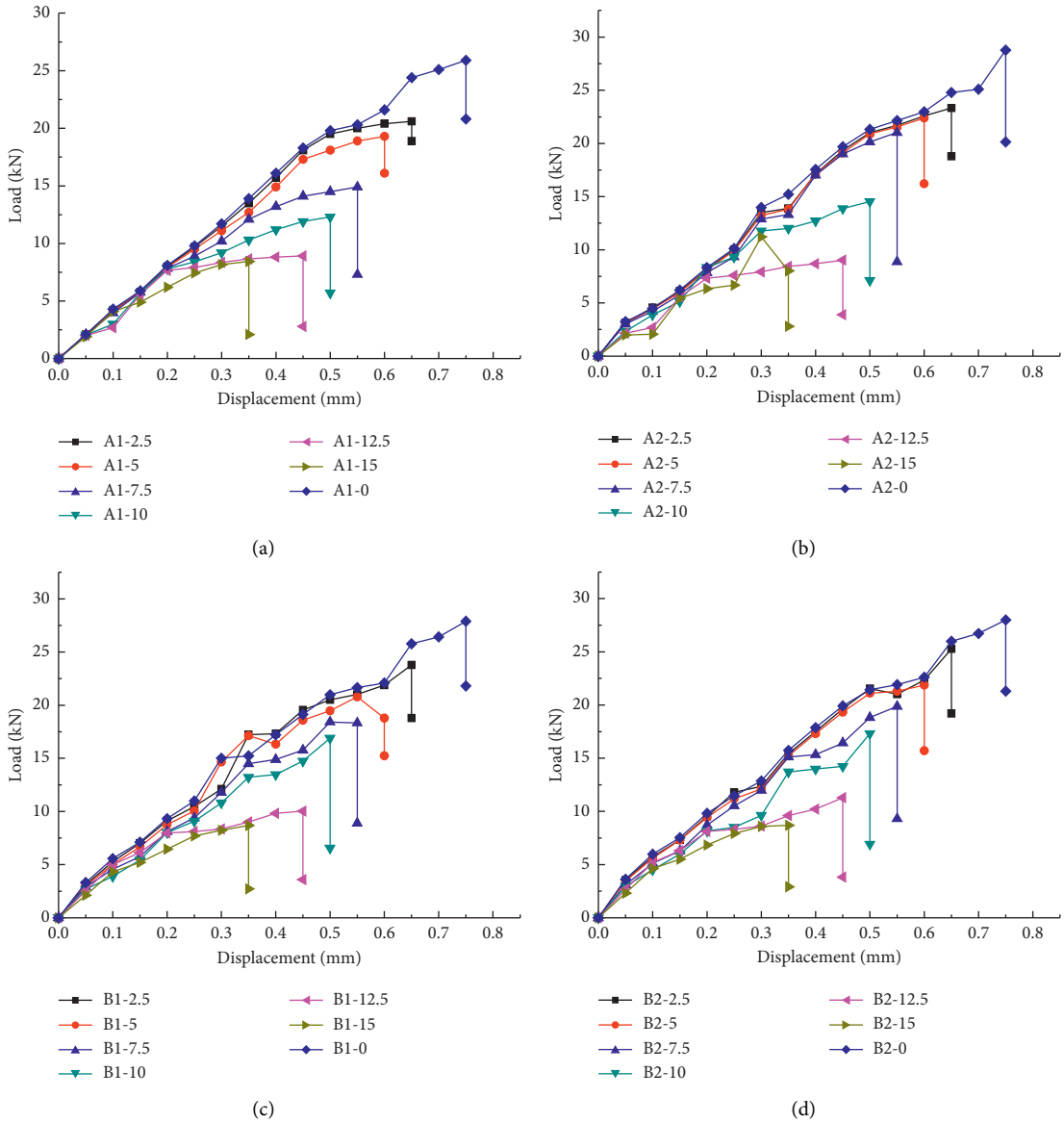

Figure 10: Continued.

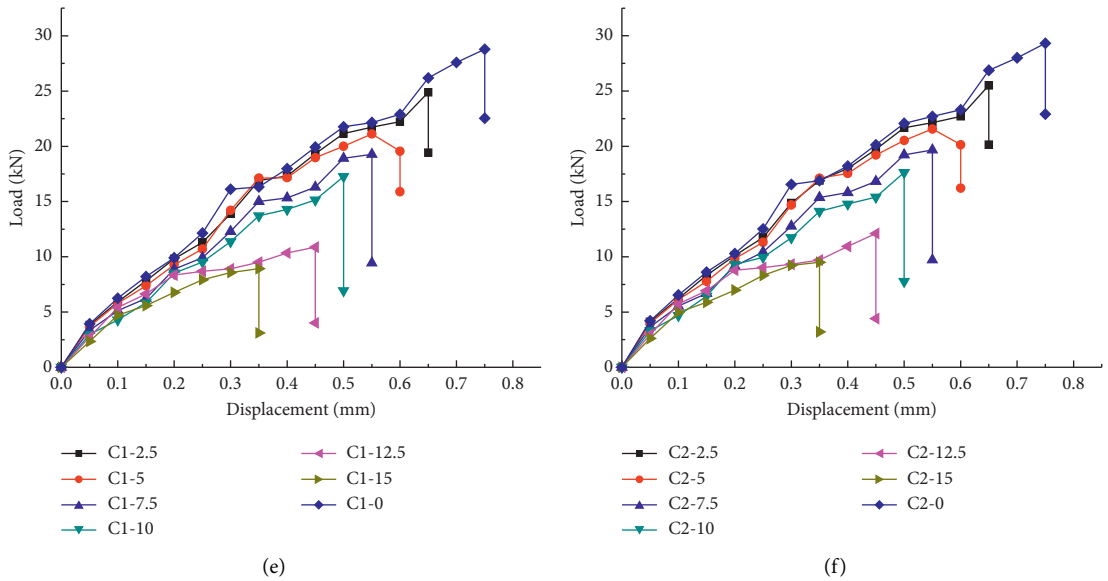

Figure 10: Load-displacement of the CFRP-steel plate specimens. (a) One-layer CFRP with width of 30 mm. (b) Two-layer CFRP with width of 30 mm. (c) One-layer CFRP with width of 40 mm. (d) Two-layer CFRP with width of 40 mm. (e) One-layer CFRP with width of 50 mm. (f) Two-layer CFRP with width of 50 mm.

the CFRP sheets was 30 mm, the difference of the maximum bond forces was not obvious at low corrosion degrees of 0% and 2.5%. When the number of CFRP layers increased from one to two, the ultimate bond strength increased by 16%, 19%, and 32% at corrosion degrees of 5%, 10%, and 15%, respectively. However, the ultimate displacement of specimen A2-15 was approximately 0.05 mm smaller than that of specimen A1-15 at a corrosion of 15%. The number of CFRP layers had a significant effect on the bond strength, while it had a small effect on the ultimate displacement with the growth of the corrosion degree.

For the CFRP sheets with widths of 40 mm and 50 mm, the maximum bond strength also decreased rapidly as the corrosion degree increased. The maximum bond strength increased when the number of CFRP sheet layers changed from one to two for the same CFRP sheet width. The test results showed that the rule of the maximum bond strength change was similar to that for a CFRP sheet width of 30 mm. The CFRP sheet could seal the pile specimens and isolate them from the corrosive medium that would destroy the adhesive interface of the CFRP and steel tubes. Maintaining the adhesive interface in a good condition was important to making full use of the restraining force of the CFRP to enhance CFRP-CFST pile load capacity. The CFRP sheet could not only increase the load capacity but also prevent the material from corroding compared with the CFST pile with no outer CFRP sheet.

4. Conclusions

This paper presents the results of a test program that investigated the resistance to corrosion of CFRP-CFST pile specimens subjected to a simulated hygrothermal environment. Based on the experimental results of this study, the following conclusions were drawn.

The CFRP sheet of the CFRP-CFST pile specimens could seal the surface of the piles and prevent further ingression of harmful substances into the pile. Piles provided excellent protection against corrosion in terms of their corrosion strain, half-cell potential, corrosion products, and adhesive property as the number of CFRP layers increased.

The dry and wet alternating zone was the most serious corrosion zone because it was wetted periodically by the tidal level and had sufficient oxygen and water. The average potential was smaller than that of the other two corrosion zones. The half-cell potential of the piles decreased as the number of CFRP sheet layers increased, especially at high corrosion degrees. Two layers of externally bonded CFRP sheets in the tidal range zone reduced the corrosion activity by up to 45% and 52% compared with one and no CFRP sheets, respectively, at a corrosion degree of 15%.

The accumulation of products would produce the expansion stress that caused surface strain of the CFRP-CFST pile specimens. The CFRP sheet of the CFRP-CFST pile specimens could prevent the penetration of the corrosive medium, which delayed the corrosion of the pile. The strains of the piles decreased as the number of CFRP sheet layers increased. The higher the lever of the corrosion degree, the clearer the effects.

The corresponding components of the corrosion products were mainly Fe_2O_3, Fe_3O_4, α- FeOOH, and γ-FeOOH by diffraction peaks. It was also concluded that the number of diffraction peaks decreased as the number CFRP sheet layers increased. This indicated that an increase in the number of CFRP sheet layers could slow the corrosion degree of the pile specimens because the CFRP sheet prevented the invasion of the aggressive medium.

The CFRP sheet could not only increase the load capacity but also prevent the material from corroding. The maximum bond force decreased as the corrosion degree increased.

When the number of CFRP layers increased from one to two, the ultimate bond strength increased by 16%, 19%, and 32% at corrosion degrees of 5%, 10%, and 15%, respectively. The number of CFRP layers had a significant effect on the bond strength, while it had little effect on the ultimate displacement with the growth of the corrosion degree.

Data Availability

The data used to support the findings of this study are included within the article.

Conflicts of Interest

The authors declare that they have no conflicts of interest.

Acknowledgments

The research was financially supported by National Natural Science Foundation of China (51679080 and 51379073) and Natural Science Foundation of Jiangsu Province (BK20131371).

References

[1] M. C. Sundarraja and S. Rajamohan, "Strengthening of RC beams in shear using GFRP inclined strips—an experimental study," *Construction and Building Materials*, vol. 23, no. 2, pp. 856–864, 2009.

[2] E. P. Najafabadi, M. H. Khaneghahi, H. A. Amiri, H. E. Estekanchi, and T. Ozbakkaloglu, "Experimental investigation and probabilistic models for residual mechanical properties of GFRP pultruded profiles exposed to elevated temperatures," *Composite Structures*, vol. 211, pp. 610–629, 2019.

[3] M. Bazli, H. Ashrafi, A. Jafari, X.-L. Zhao, H. Gholipour, and A. V. Oskouei, "Effect of thickness and reinforcement configuration on flexural and impact behaviour of GFRP laminates after exposure to elevated temperatures," *Composites Part B: Engineering*, vol. 157, pp. 76–99, 2019.

[4] K. A. Soudki and T. G. Sherwood, "Behaviour of reinforced concrete beams strengthened with carbon fibre reinforced polymer laminates subjected to corrosion damage," *Canadian Journal of Civil Engineering*, vol. 27, no. 5, pp. 1005–1010, 2000.

[5] Y. Wei, G. Wu, Z. S. Wu, and D. S. Gu, "Flexural behavior of concrete-filled FRP-steel composite circular tubes," *Advanced Materials Research*, vol. 243–249, pp. 1316–1320, 2011.

[6] F. Duprat, "Reliability of RC beams under chloride-ingress," *Construction and Building Materials*, vol. 21, no. 8, pp. 1605–1616, 2007.

[7] N. Grace, T. Enomoto, P. Baah, and M. Bebawy, "Flexural behavior of CFRP precast prestressed decked bulb T-beams," *Journal of Composites for Construction*, vol. 16, no. 3, pp. 225–234, 2012.

[8] M. Faruqi and M. S. Khan, "Deflection behavior of a prestressed concrete beam reinforced with carbon fibers at elevated temperatures," *Frontiers of Structural and Civil Engineering*, vol. 13, no. 1, pp. 81–91, 2019.

[9] P. A. Nguyen, T. T. Banh, D. Lee, J. Lee, J. Kang, and S. Shin, "Design of multiphase carbon fiber reinforcement of crack existing concrete structures using topology optimization," *Steel and Composite Structures*, vol. 29, pp. 635–645, 2018.

[10] A. C. Thomas and K. Baskar, "Testing and evaluation of bond surface profile influencing the CFRP strengthening of steel members," *Journal of Testing and Evaluation*, vol. 46, no. 6, pp. 2569–2583, 2018.

[11] M. G. Sohail, S. Laurens, F. Deby, and J. P. Balayssac, "Significance of macrocell corrosion of reinforcing steel in partially carbonated concrete: numerical and experimental investigation," *Materials and Structures*, vol. 48, no. 1-2, pp. 217–233, 2015.

[12] E. Sassine, S. Laurens, R. François, and E. Ringot, "A critical discussion on rebar electrical continuity and usual interpretation thresholds in the field of half-cell potential measurements in steel reinforced concrete," *Materials and Structures*, vol. 51, p. 93, 2018.

[13] R. Zhang, A. Castel, and R. François, "The corrosion pattern of reinforcement and its influence on serviceability of reinforced concrete members in chloride environment," *Cement and Concrete Research*, vol. 39, no. 11, pp. 1077–1086, 2009.

[14] L. Sadowski, "Methodology for assessing the probability of corrosion in concrete structures on the basis of half-cell potential and concrete resistivity measurements," *The Scientific World Journal*, vol. 2013, Article ID 714501, 8 pages, 2013.

[15] R. Capozucca and S. Bossoletti, "Static and free vibration analysis of RC beams with NSM CFRP rectangular rods," *Composites Part B: Engineering*, vol. 67, pp. 95–110, 2014.

[16] B. H. Osman, E. Wu, B. Ji, and S. S. Abdulhameed, "Effect of reinforcement ratios on shear behavior of concrete beams strengthened with CFRP sheets," *HBRC Journal*, vol. 14, p. 29, 2018.

[17] G. Przemyslaw and S. Tomasz, "A novel application of alumina fiber mats as TBC protection for CFRP/epoxy laminates –Laboratory tests and numerical modeling," *Journal of the European Ceramic Society*, vol. 38, no. 8, pp. 2920–2927, 2018.

[18] J. H. Park, B. W. Jo, S. J. Yoon, and S. K. Park, "Experimental investigation on the structural behaviour of concrete filled FRP tubes with/without steel rebar," *KSCE Journal of Civil Engineering*, vol. 15, no. 2, pp. 337–345, 2011.

[19] A. Davol, R. Burgueño, and F. Seible, "Flexural behavior of circular concrete filled FRP shells," *Journal of Structural Engineering*, vol. 127, no. 7, pp. 810–817, 2001.

[20] M. Afifi, H. Mohamed, and B. Benmokrane, "Axial capacity of circular concrete columns reinforced with GFRP bars and spirals," *Journal of Composites for Construction*, vol. 18, no. 1, 2014.

[21] S. S. Faza and H. V. S. Gangarao, "Pre and post-cracking deflection behaviour of concrete beams reinforced with fibre-reinforced plastic rebars," in *Proceedings of 1992 1st International Conference on Advanced Composite Materials in Bridges and Structures*, p. 151, Sherbrooke, Canada, 1992.

[22] F. Debieb, L. Courard, S. Kenai, and R. Degeimbre, "Mechanical and durability properties of concrete using contaminated recycled aggregates," *Cement and Concrete Composites*, vol. 32, no. 6, pp. 421–426, 2010.

[23] M. N. S. Hadi, T. M. Pham, and X. Lei, "New method of strengthening reinforced concrete square columns by circularizing and wrapping with fiber-reinforced polymer or steel straps," *Journal of Composites for Construction*, vol. 17, no. 2, pp. 229–238, 2013.

[24] M. Vasumathi and V. Murali, "Effect of alternate metals for use in natural fibre reinforced fibre metal laminates under bending, impact and axial loadings," *Procedia Engineering*, vol. 64, pp. 562–570, 2013.

[25] Y. Pan, G. Wu, X. Cheng et al., "Galvanic corrosion behaviour of carbon fibre reinforced polymer/magnesium alloys coupling," *Corrosion Science*, vol. 98, pp. 672–677, 2015.
[26] J. Zhang and C. Wu, "Corrosion protection behavior of AZ31 magnesium alloy with cathodic electrophoretic coating pretreated by silane," *Progress in Organic Coatings*, vol. 66, no. 4, pp. 387–392, 2009.
[27] V. Yazici and M. N. Hadi, "Axial load-bending moment diagrams of carbon FRP wrapped hollow core reinforced concrete columns," *Journal of Composites for Construction*, vol. 13, no. 4, pp. 262–268, 2009.
[28] H. M. Mohamed and R. Masmoudi, "Flexural strength and behavior of steel and FRP-reinforced concrete-filled FRP tube beams," *Engineering Structures*, vol. 32, no. 11, pp. 3789–3800, 2010.
[29] M. N. S. Hadi, W. Wang, and M. N. Sheikh, "Axial compressive behaviour of GFRP tube reinforced concrete columns," *Construction and Building Materials*, vol. 81, pp. 198–207, 2015.
[30] A. Yoshimura, T. Nakao, S. Yashiro, and N. Takeda, "Improvement on out-of-plane impact resistance of cfrp laminates due to through-the-thickness stitching," *Composites Part A: Applied Science and Manufacturing*, vol. 39, no. 9, pp. 1370–1379, 2008.
[31] X. Han, S. Hou, L. Ying, W. Hou, and H. Aliyev, "On the fracture behaviour of adhesively bonded CFRP hat-shaped thin-walled beam under axial crushing load: an experimental and modelling study," *Composite Structures*, vol. 215, pp. 258–265, 2019.
[32] H. A. M. Araújo, J. J. M. Machado, E. A. S. Marques, and L. F. M. da Silva, "Dynamic behaviour of composite adhesive joints for the automotive industry," *Composite Structures*, vol. 171, pp. 549–561, 2017.
[33] M. Burley, J. E. Campbell, J. Dean, and T. W. Clyne, "Johnson-cook parameter evaluation from ballistic impact data via iterative fem modelling," *International Journal of Impact Engineering*, vol. 112, pp. 180–192, 2018.